CHEMBIOCHEM

# Supporting Information



# A Single-Stranded Junction Modulates Nanosecond Motional Ordering of the Substrate Recognition Duplex of a Group I Ribozyme

Phuong Nguyen,[a] Xuesong Shi,[b] Snorri Th. Sigurdsson,[c] Daniel Herschlag,[b] and Peter Z. Qin*[a]

cbic_201300376_sm_miscellaneous_information.pdf

## Section S.1: Materials and Methods

### RNA preparation

The *Tetrahymena* group I ribozyme used in this study was the L-16 *ScaI* variant,[1] with the wild type ribozyme having an 11-base-pair P1 duplex connected to the core by a three-nucleotide single-stranded J1/2 junction (Figure S1).

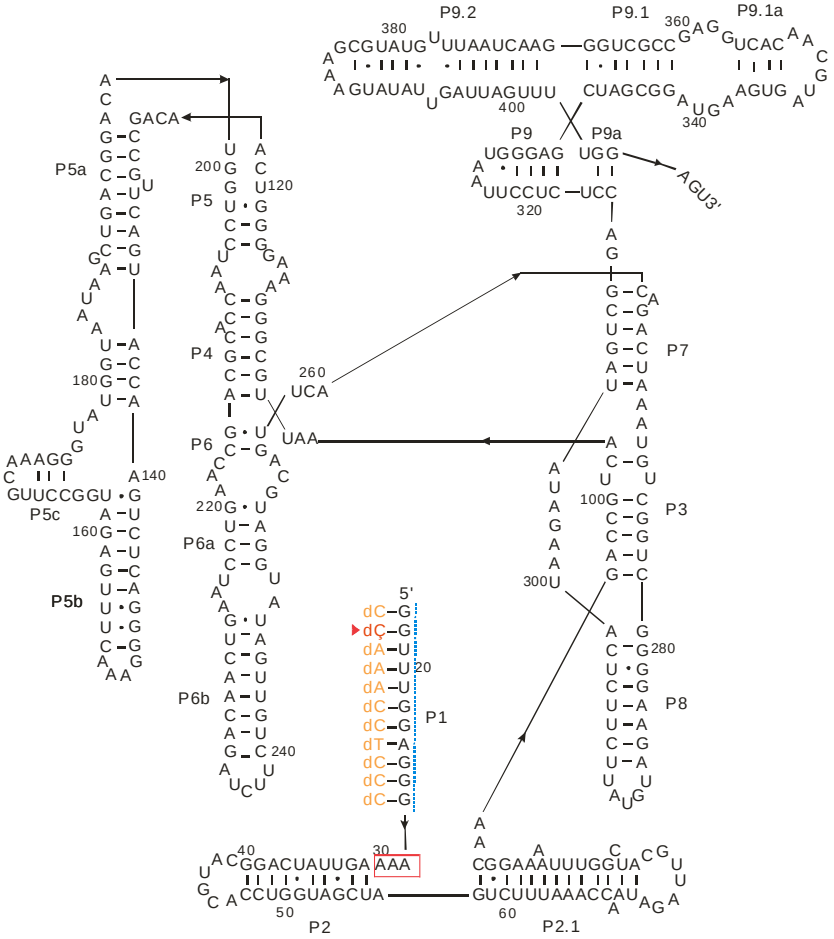


**Figure S1:** Secondary structure of the group I ribozyme construct. A deoxyribose-oligonucleotide analogue of the oligonucleotide substrate (orange) base-pairs with the Internal Guide Sequence (blue dotted region) to form the P1 duplex, which is connected to the ribozyme core through the single-stranded J1/2 junction (red box).

All ribozyme variants were prepared by *in vitro* transcription using linearized double-stranded DNA templates,[1] which were generated by PCR from a plasmid containing the wild type ribozyme using appropriate primers (Table S1). The PCR products were purified using Qiaquick columns (Qiagen), and were verified by sequencing. Each transcription reaction was carried out using the appropriate DNA template (5μg/mL), 4 mM $MgCl_2$, 0.5 mM NTPs, 40 mM DTT, 40 mM Tris·HCl, pH 8.1, 0.01% Triton X-100, 2 mM Spermidine, and T7 RNA polymerase. Transcription was allowed to proceed at 30 °C for 40 min, and the product was recovered by ethanol precipitation and then purified by RNeasy columns (Qiagen). The quality of column-purified RNA was confirmed by denaturing polyacrylamide gel electrophoresis and estimated to be at least 95% pure. The concentration for each ribozyme was determined by its absorbance at 260 nm using an extinction coefficient of $3.25 \times 10^6$ $M^{-1}cm^{-1}$.

**Table S1.** List of PCR primers for generating DNA templates for different ribozyme variants

| Forward primer | |
|---|---|
| Ribozyme | |
| 0-nt | 5'-GCGCTTAATACGACTCACTATAGGTTTGGAGG GAGTTATCAGGCATGC-3' |
| 3A (wild-type) | 5'-GCGCTTAATACGACTCACTATAGGTTTGGAGG G**AAA**AGTTATCAGGCATGC-3' |
| 5A | 5'-GCGCTTAATACGACTCACTATAGGTTTGGAGG G**AAAAA**AGTTATCAGGCATGC-3' |
| 8A | 5'-GCGCTTAATACGACTCACTATAGGTTTGGAGG G**AAAAAAAA**AGTTATCAGGCATGC-3' |
| 3U | 5'-GCGCTTAATACGACTCACTATAGGTTTGGAGG G**TTT**AGTTATCAGGCATGC-3' |
| 5U | 5'-GCGCTTAATACGACTCACTATAGGTTTGGAGG G**TTTTT**AGTTATCAGGCATGC-3' |
| 8U | 5'-GCGCTTAATACGACTCACTATAGGTTTGGAGG G**TTTTTTTT**AGTTATCAGGCATGC-3' |
| Reverse primer | |
| | 5'-ACTCCAAAACTAATCAATATACTTTCGC-3' |

The dS$^{\text{Ç}}$ oligonucleotide (5'-dCdCdCdTdCdCdAdAdAd**Ç**dC-3'), in which the 10$^{th}$ nucleotide is substituted by **Ç**, was synthesized as reported.[2] All other oligonucleotides were obtained commercially from Integrated DNA Technologies, Inc. (Coralville, Iowa) and were purified by HPLC.[3]

The use of a deoxyribose-oligonucleotide substrate analogue (dS$^{\text{Ç}}$) favors the open complex, i.e., one in which the P1 duplex is not docked into tertiary interactions with the ribozyme's core.[4] Based on prior studies,[5] a P1 duplex assembled with the DNA substrate dS$^{\text{Ç}}$ is expected to result in an equilibrium constant $K_{dock}$ of 0.012 between the docked and undocked states (i.e., the closed and open complex, respectively), with >98.8% of the ribozyme population in the undocked state. This conclusion is further supported by control experiments showing that under saturation conditions, active wild type 3A ribozyme, which is expected to have the highest propensity to adopt the docked state,[6] did not cleave dS$^{\text{Ç}}$ after an 8-hour incubation at 25 ºC. Substantial cleavage would be expected in less than an hour if dS$^{\text{Ç}}$ were significantly docked.[4]

## Assembly of Ç-labeled ribozyme-substrate complexes

To assemble ribozyme-substrate complexes for EPR measurements, appropriate ribozymes (300 µL of 1µM) were pre-folded at 50 °C for 30 min in buffer A (50 mM NaMOPS, pH 6.8, and 10 mM $MgCl_2$). An appropriate amount of dS$^{\text{Ç}}$ in buffer A was then added to the pre-folded ribozyme to achieve a 1 to 1.1 dS$^{\text{Ç}}$/ribozyme ratio. The mixture was incubated at room temperature for 30 minutes, then concentrated to an approximately 10-20 µL EPR-ready sample by filtering through a membrane concentrator (Millipore Inc, MWCO 30kD). The assembled substrate-ribozyme complex was immediately used for EPR measurements. The final concentration of each EPR sample ranged from 10 to 40 µM as determined by their respective absorbance at 260 nm. Based on the nearest-neighbor model[7] and prior group I ribozyme studies,[8] the dissociation constant ($K_d$) between dS$^{\text{Ç}}$ and the ribozyme was estimated to be 0.13 nM or

lower. The concentration of ribozyme/dS$^{\text{Ç}}$ complex is four orders of magnitude above this $K_d$, which should result in complete dS$^{\text{Ç}}$ binding. This conclusion is further supported by the EPR spectra (see S.2).

**Continuous-wave EPR spectroscopy**

EPR samples prepared as described above were placed in glass capillaries (1.0 × 1.2 mm) sealed at one end. X-band (~9.8 GHz) EPR spectra were acquired using a Bruker EMX Spectrometer equipped with a high sensitivity cavity (ER 4119 HS, Bruker Biospin, Inc.). The incident microwave power was 2 mW, the 100-kHz field modulation was set at 1 – 4 G depending on the central line width of the corresponding EPR samples, and sample temperature was maintained using a liquid nitrogen variable temperature setup. For each spectrum, 60-100 scans were collected and averaged, with data collection time ranging from 2 to 6 hours. Baseline correction and spectral normalization were carried out as described.[9] For the 5A ribozyme samples only, the measured EPR spectra showed a small mobile component (<5% of total spin population), which resembles that of the unbound dS$^{\text{Ç}}$. This mobile component, which is clearly distinct from that of the ribozyme bound spectrum, was subtracted using the experimentally measured unbound dS$^{\text{Ç}}$ spectrum (see example in S.2). Repeat measurements showed that variations in the measured hyperfine splitting ($2A_{eff}$) for a given sample are less than 0.30 G.

**EPR Spectral simulation**

Simulations were carried out with the EPRLL program suite using the microscopic-order-macroscopic-disorder model (MOMD).[10] A LabView based variant of the program, kindly provided by the Hubbell group from UCLA, was used throughout this work. All simulations used a previously reported set of $\boldsymbol{g}$ and $\boldsymbol{A}$ tensor values ($g_x$ = 2.0086, $g_y$ = 2.0064, $g_z$ = 2.0026, $A_x$ = 5.81 Gauss, $A_y$ = 5.75 Gauss, $A_z$ = 36.75 Gauss).[11] In addition, the allowed MOMD orientation ($N_{nort}$ = 15) and basis set truncation parameters ($L_{emx}$ = 20, $L_{omx}$ = 19, $K_{mx}$ = 8, $M_{mx}$ = 2, $IPN_{mx}$ = 2) were kept invariant. The diffusion tilt angle ($\beta_D$) was set at the optimized value of 24° (see S.6), which generates acceptable fits for all samples. Variable parameters are the rotational diffusion rate that is treated as isotropic ($R_{bar}$), the orienting potential coefficient ($C_{20}$, see below), the Gaussian inhomogeneous broadening parameter ($\Delta^{(0)}$), and the Lorentzian inhomogeneous line-broadening tensor (W) (see [10] for detailed descriptions of these parameters). In each simulation, the variable parameters were searched to yield the best-fit spectrum with the lowest mean-square-deviation ($\chi^2$) value as compared to the measured one.[10]

In all simulations reported, the orienting potential U(θ) was expressed as:

$$U(\theta) = -\frac{1}{2}(k_B T)C_{20}(3\cos^2\theta - 1) \qquad (1)$$

where θ is the angle between the instantaneous and the overall-averaged nitroxide diffusion axes, $k_B$ is the the Boltzmann constant, T is the temperatature, and $C_{20}$ is a coefficient that may be varied during simulation.The order parameter S is computed from U(θ):[10]

$$S = <\frac{3\cos^2\theta - 1}{2}> = \frac{\int \frac{1}{2}(3\cos^2\theta - 1)\exp\left(-\frac{U(\theta)}{k_B T}\right)\sin(\theta)d\theta}{\int \exp\left(-\frac{U(\theta)}{k_B T}\right)\sin(\theta)d\theta} \qquad (2)$$

From S, a quantity defined as $\theta_r$ was computed as:

$$\theta_r = \cos^{-1}\left(\sqrt{\frac{2S+1}{3}}\right) \quad (3)$$

$\theta_r$ represents an effetive amplitude for the rotational motion of the nitroxide.[12]

## Section S.2: Additional spectra of dS$^{C}$

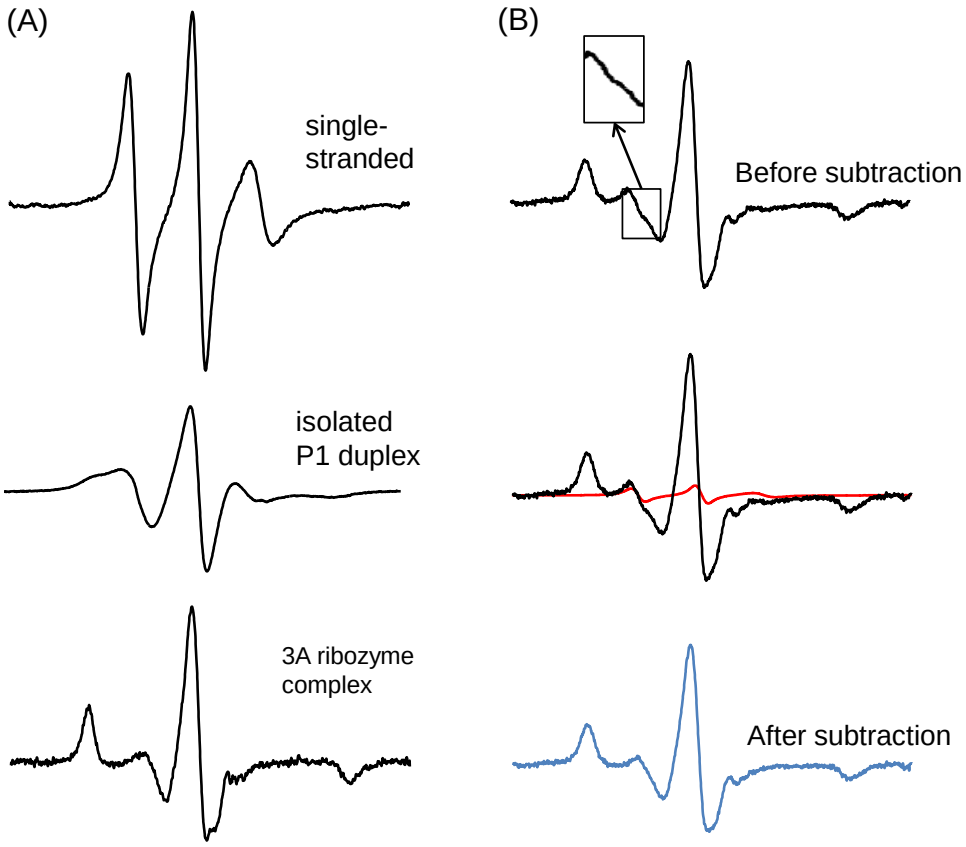


**Figure S2:** (A) X-band cw-EPR spectra of dS$^{C}$ assembled into various species. The spectra were measured in buffer A (50 mM NaMOPS, pH 6.8, and 10 mM $MgCl_2$) at 25 ºC. The single-stranded dS$^{C}$ spectrum (top) shows three sharp lines, which are characteristics of a nitroxide undergoing isotropic tumbling. This is distinct from that of the isolated P1 duplex (middle) and that assembled with the 3A (wild-type) ribozyme (bottom). Also note that in the 3A spectrum there is no indication of any mobile components corresponding to that of single-stranded dS$^{C}$, indicating complete binding of dS$^{C}$ by the ribozyme. (B) An example of mobile component subtraction. The 25 °C 5A ribozyme spectrum with a very small mobile component (inset) is shown in the top panel. To remove this mobile component, the measured single-stranded dS$^{C}$ spectrum (red) was scaled to 5% of the total spin population (middle panel) and subtracted from the measured ribozyme spectrum (bottom panel).[9] Note that this operation does not affect the high- and low-field peaks.

**Section S.3: Invariant EPR spectra observed upon altering Ç location within P1**

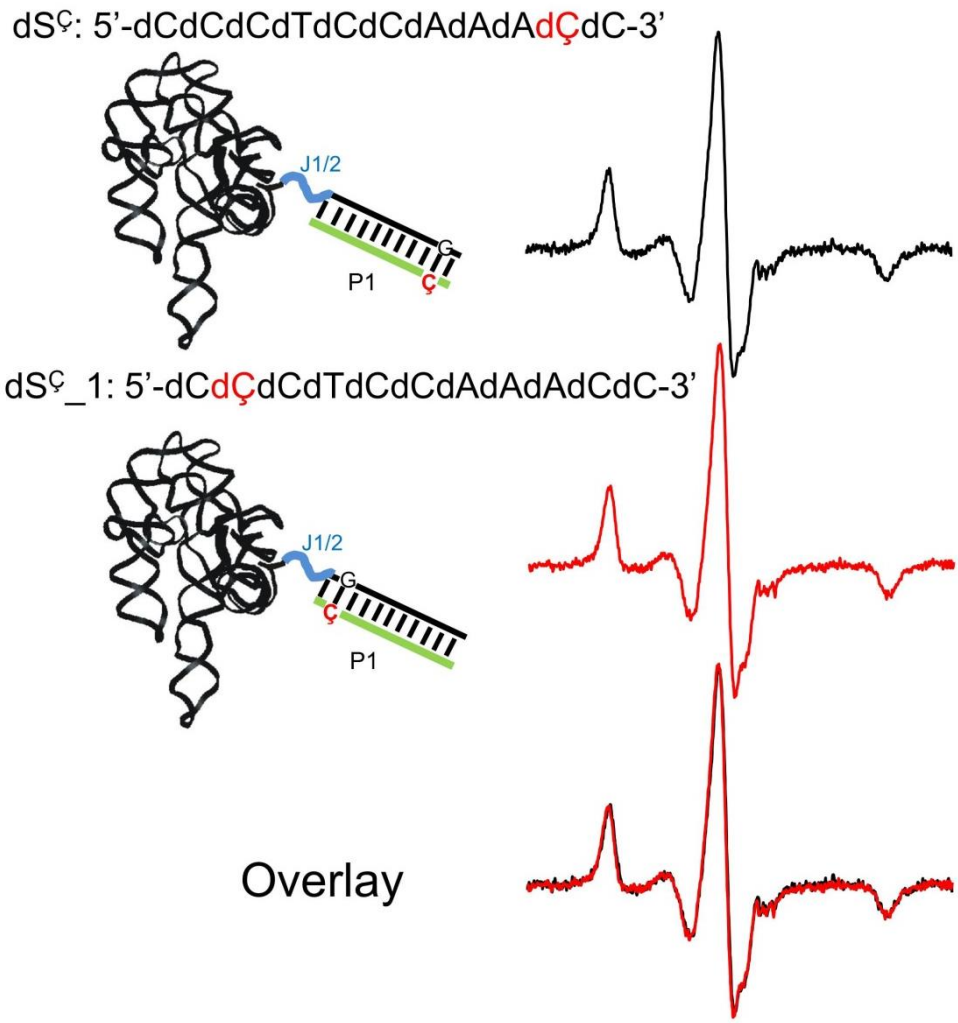


**Figure S3:** Spectral comparisons between two substrate analogues with different **Ç** locations. Spectra were obtained in buffer A (50 mM NaMOPS, pH 6.8, and 10 mM $MgCl_2$) at 25 ºC using the 3A (wild-type) ribozyme.

**Section S.4: Spectral comparisons between ribozymes with different J1/2 sequences**

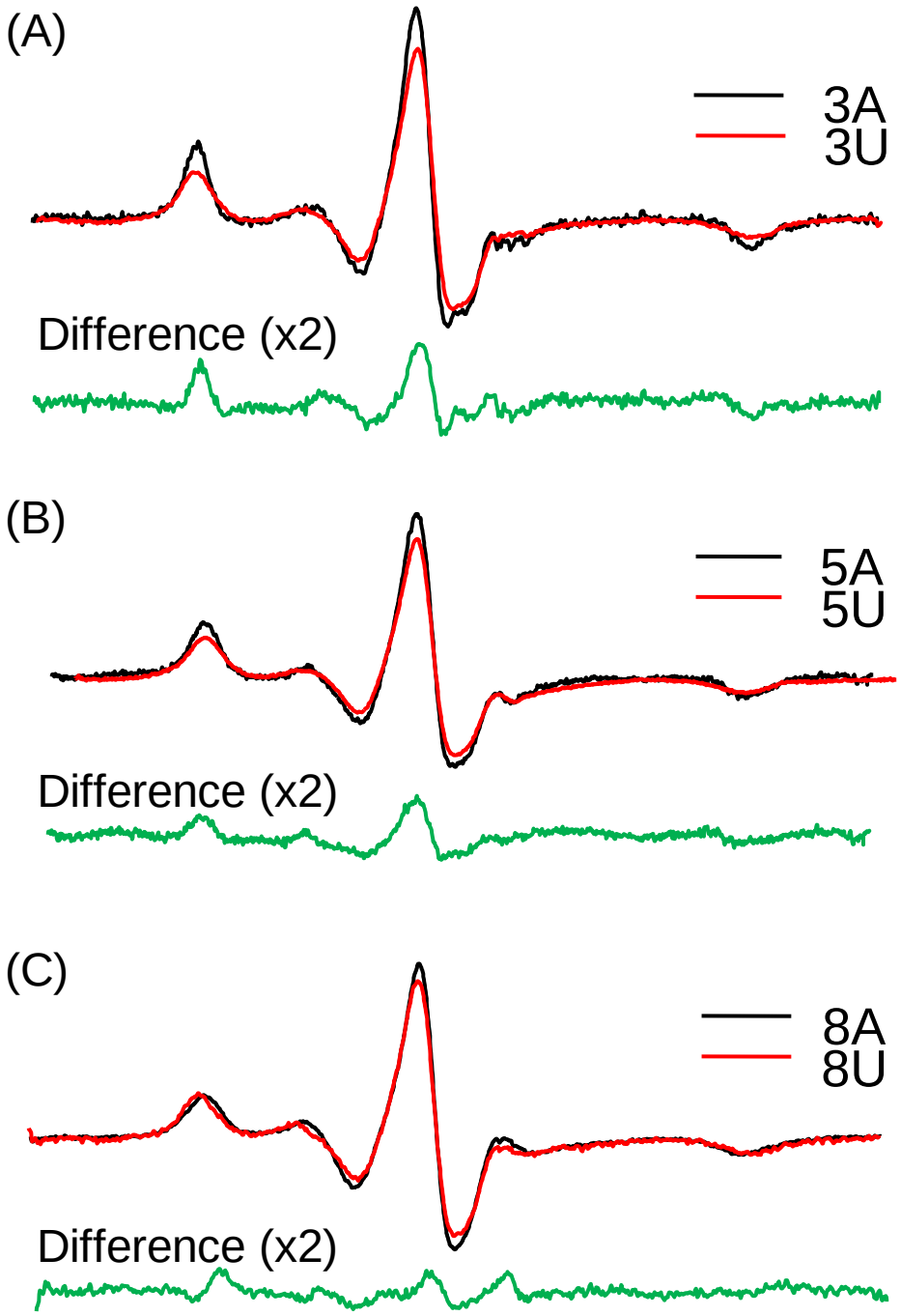


**Figure S4:** Comparisons between aqueous **Ç** spectra of the open complex for ribozyme variants of varying J1/2 sequence at three specific J1/2 lengths. Spectra were obtained in buffer A (50 mM NaMOPS, pH 6.8, and 10 mM $MgCl_2$) at 25 ºC. The amplitude of the difference spectra were scaled by 2-fold.

**Section S.5: Spectral comparisons between the 3A and 3U ribozymes**

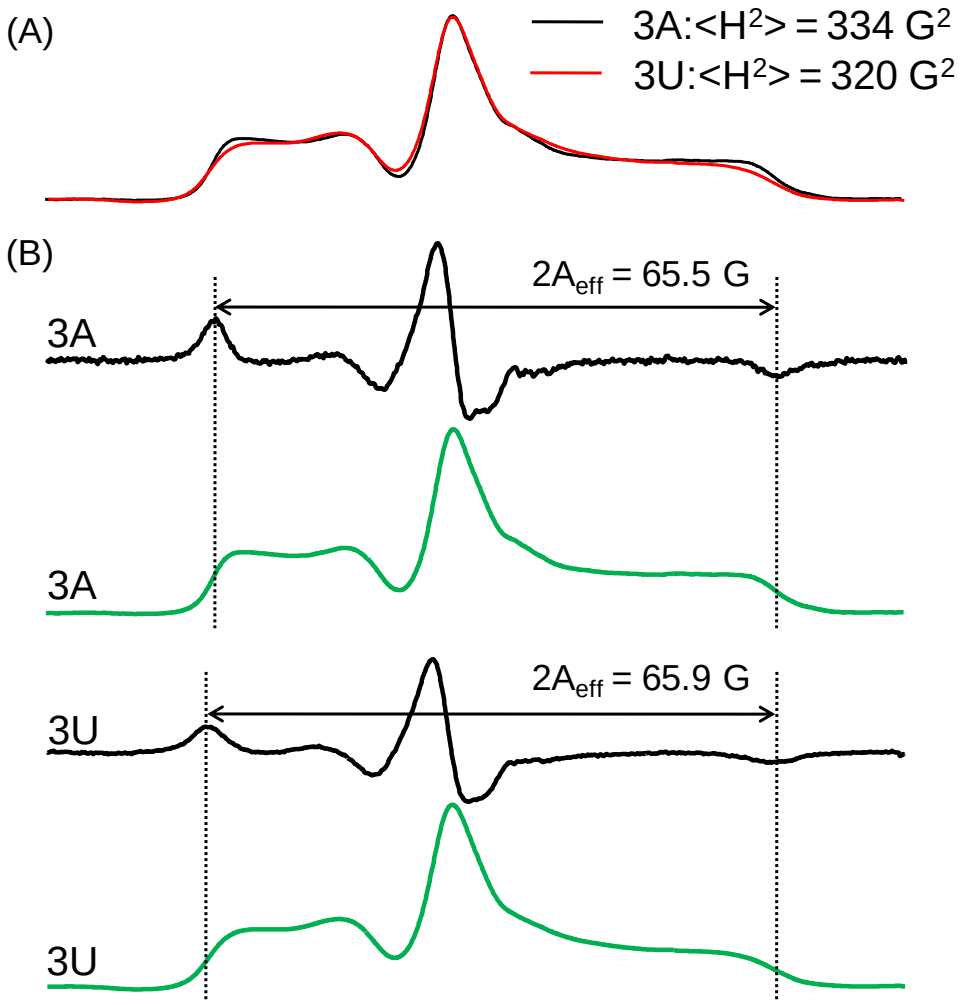


**Figure S5**: (A) Comparisons between normalized EPR absorption spectra of the 3A and 3U ribozymes. The absorption spectra were obtained by integrating the experimentally measured EPR spectrum, which represents the first derivative of the absorption spectrum due to the use of the phase sensitive detection scheme.[9] As compared to the 3U spectrum, the 3A spectrum shows more prominent outer shoulders and a larger spectral breath as measured by the spectral second moment ($<H^2>^{[13]}$). (B) Connecting the variations in the absorption spectra to the effective hyperfine splitting ($2A_{eff}$). The $2A_{eff}$ value is measured between the two outer maxima of the experimentally measured spectra (black). The outer maxima correponds to the point with the steepest slope at the outedge of the absorption spectrum (green). The slopes at the outer edges of integrated spectra differ between the 3A and 3U ribozymes, giving rise to a slightly smaller $2A_{eff}$ in the 3A spectrum.

**Section S.6: Supplemental data and discussion on EPR spectral simulations**

*S6.1. Parameters for the simulated best-fit spectra*[a]

| Ribozyme | | 0-nt | 3A[b] | 3U[b] | 5A | 5U | 8A | 8U |
|---|---|---|---|---|---|---|---|---|
| ordering potential | **$C_{20}$**[c] | **8.50** | **8.01** | **3.17** | **3.36** | **2.88** | **2.46** | **2.33** |
| diffusion rate | $\log_{10}(R_{bar})$[c] | 7.75 | 7.76 | 7.26 | 7.29 | 7.30 | 7.46 | 7.38 |
| line broadening | $\Delta^{(0)}$ | 1.91 | 2.31 | 2.69 | 3.11 | 1.97 | 1.97 | 2.85 |
| | W | 0.37 | 0.10 | 0.30 | 0.42 | 0.18 | 0.17 | 0.50 |
| $\chi^2(\times 10^{-5})$ | | 8.25 | 3.77 | 3.53 | 4.38 | 3.55 | 1.33 | 2.27 |

(a) The listed parameters were simulataneously varied to obtain the best-fit spectrum (see Methods, S.1).

(b) Note that the simulations yielded a larger $C_{20}$ (i.e., higher order parameter S and a smaller amplitude of motion, see S.1) and a larger $\log_{10}(R_{bar})$ (i.e., faster rate) for the 3A ribozyme as compared to that of the 3U. Such changes of motion, i.e., "increasing ordering with increasing rate", is considered as one form of "reducing mobility". For example, in NMR studies of hemoglobin, it has been reported that "rigid" N-H bonds located in secondary structure elements have larger order parameters and faster rates as compared to flexible N-H bonds located in loops.[14]

(c) $C_{20}$ and $R_{bar}$ are known to co-very to a certain extent.[15] Effects due to such co-variation are examined in S.6.3.

*S.6.2. Assessing the effects of $\beta_D$*

$\beta_D$ is a parameter that relates the principal diffusion frame to the nitroxide magnetic frame.[10] For all samples studied here, to a first-order approximation we assume that the relationship between the diffusion frame and magnetic frame is invariant, and therefore an optimized $\beta_D$ value of 24˚was used in all simulations (see S.1, Methods). To assess how the simulations would be impacted if $\beta_D$ was allowed to vary, we simulated the 3A and the 3U spectra, which show the most differences, with varying $\beta_D$. The resulting best-fit spectrum has minimal differences as compared to that obtained with a fixed $\beta_D$ of 24.0°, with very small variation in $\beta_D$ (Figure S6.2). This suggests that the fixing $\beta_D$ at 24.0° is sufficient and does not significantly impact simulations reported here (Figure S6.2).

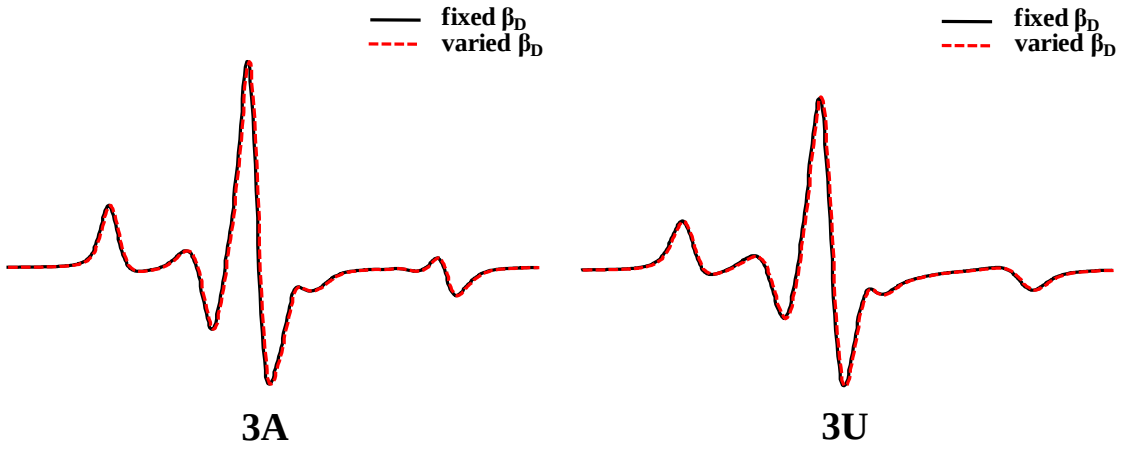


**Figure S6.2:** Comparisons of the best-fit spectra obtained with all parameters fixed at values reported in Section S.6.1, except that $\beta_D$ was varied. For either the 3A or the 3U spectrum, the resulting best-fit spectrum (dotted red traces) has minimal difference as compared to that obtained with a fixed $\beta_D$ of 24.0° (black traces), with the optimized $\beta_D$ values varied by < 10% (24.1° and 21.7° for 3A and 3U, respectively).

*S.6.3.Impacts due to co-variation of order and rate determined from spectral simulation*

A known issue in EPR simulation at a single frequency is that the simulation parameters may co-vary to a certain extent, so that different parameter sets may yield simulated spectra that fit comparably to a particular experimental spectrum.[15] The orienting potential coefficient ($C_{20}$) and the rotational diffusion rate ($R_{bar}$) have the strongest tendency to co-vary: increases in $C_{20}$ and in $R_{bar}$ have opposite effects on magnetic tensor averaging, and therefore within a certain range they may compensate each other to yield the same simulated spectrum. To assess whether the $C_{20}/R_{bar}$ co-variation could alter the conclusion that the motion detected in the 3A spectrum is more ordered, we followed a previously reported approach[15b] and examined the range of $C_{20}$ and $R_{bar}$ that yield acceptable fits to the measured 3A and 3U spectra.

Simulations were carried out in which $C_{20}$ was stepped through a range of fixed values. At each fixed $C_{20}$, the "best-fit" spectrum (i.e., that with the lowest $\chi^2$) was obtained by varying $R_{bar}$, $\Delta^{(0)}$ (the Gaussian inhomogenenous broading), and W (the Lorentzian inhomogenous line-broadening). Two criteria were then used to determine whether this "lowest-$\chi^2$" spectrum is an acceptable fit to the measured spectrum. First, the difference of the effective hyperfine splitting ($\Delta$2A) was computed between the simulated spetrum and the mesured one, with $\Delta 2A \leq 0.30$ G (0.30 G is experimental errors in EPR measurements determined from repeat measurements) set as the threhold for an acceptable fit. In addition, each set of simulated spectrum was visually inspected to assure that at the high- and low-field manifolds the simulated spectrum reproduced characteristics of the measured spectrum.

These controls show that for the 3A spectrum, acceptable fits can be obtained only if $C_{20} \geq 6$ and $\log_{10}(R_{bar}) \geq 7.54$ (Figure S.6.3a), corresponding to $S \geq 0.82$ and $R_{bar} \geq 3.47 \times 10^7$ $s^{-1}$; while for the 3U spectrum, $C_{20} \leq 4$ and $\log_{10}(R_{bar}) \leq 7.32$ (Figure S6.3b), corresponding to $S \leq 0.71$ and $R_{bar} \leq 2.09 \times 10^7$ $s^{-1}$. These results support the description that motion detected in the 3A spectrum is more ordered with a faster rate, although the difference in rate may be small. A similar conclusion was also obtained in control simulations where the rate ($R_{bar}$) was stepped through a range of fixed values.

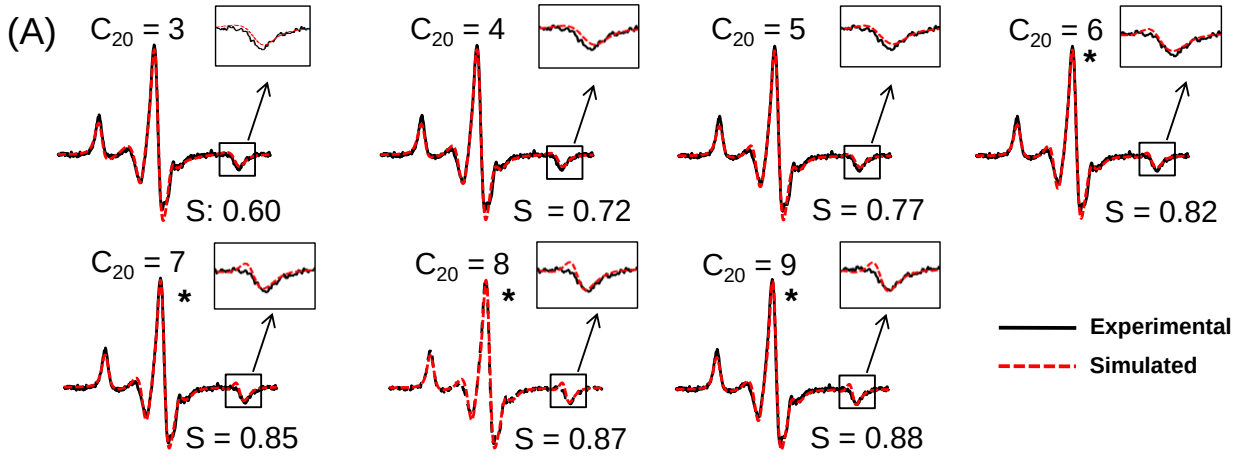


(B) Parameters for the simulated spectra reported above

| | | | | | | | | | |
|---|---|---|---|---|---|---|---|---|---|
| Fitting Parameters | ordering potential | $C_{20}$ | 3 | 4 | 5 | 6 | 7 | 8 | 9 |
| | | S | 0.60 | 0.71 | 0.77 | 0.82 | 0.85 | 0.87 | 0.88 |
| | diffusion rate | $\log_{10}(R_{bar})$ | 7.16 | 7.23 | 7.37 | 7.54 | 7.66 | 7.76 | 7.83 |
| | | $R_{bar}$ ($x10^7$ $s^{-1}$) | 1.45 | 1.70 | 2.34 | 3.47 | 4.57 | 5.75 | 6.76 |
| | line broadening | $\Delta^{(0)}$ | 1.63 | 2.14 | 2.33 | 2.22 | 2.19 | 2.24 | 2.31 |
| | | W | 0.21 | 0.19 | 0.07 | 0.09 | 0.11 | 0.11 | 0.09 |
| Criteria Matrix | | $\Delta 2A$ [(a)] | 0.92 | 1.11 | 0.71 | 0.06 | 0.03 | 0.14 | 0.28 |

(a) $\Delta 2A = |2A_{eff}' - 2A_{eff}|$, where the $2A_{eff}'$ is measured from the simulated spectrum and the $2A_{eff}$ is directly measured from the experimental spectrum, in this case, $2A_{eff}$ = 65.48 Gauss

**Figure S6.3a:** Simulation of the 3A spectrum obtained at 25 °C. (A) Comparison of the "lowest-$\chi^2$" spectra (dotted red) to that of the measured one (black). Each "lowest-$\chi^2$" spectrum was simulated with a fixed $C_{20}$ as indicated. (B) Simulation parameters and assessement matrics for "lowest-$\chi^2$" spectra shown in (A). Sets marked by "*"were deemed acceptable based on criteria described in S.6.3. The other three sets either give $\Delta 2A > 0.30$ G, and/or show clear deviations at the high-field manisfold (inset), and therefore were deemed not acceptable. Overall, the analyses indicate that for the 3A spectrum, $C_{20}$ must be greater than 6 ($S \geq 0.82$) and correspondingly $\log_{10}(R_{bar}) \geq 7.54$.

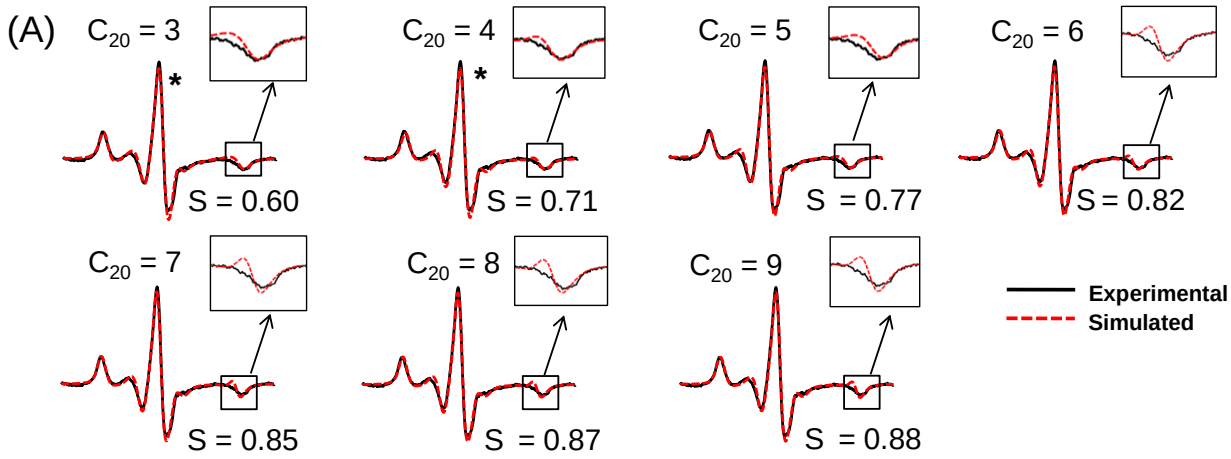


(B) Parameters for the simulated spectra reported above

| | | | | | | | | | |
|---|---|---|---|---|---|---|---|---|---|
| Fitting Parameters | ordering potential | $C_{20}$ | 3 | 4 | 5 | 6 | 7 | 8 | 9 |
| | | S | 0.60 | 0.71 | 0.77 | 0.82 | 0.85 | 0.87 | 0.88 |
| | diffusion rate | $\log_{10}(R_{bar})$ | 7.25 | 7.32 | 7.49 | 7.65 | 7.77 | 7.87 | 7.93 |
| | | $R_{bar}$ ($x10^7$ $s^{-1}$) | 1.78 | 2.09 | 3.09 | 4.47 | 5.89 | 7.41 | 8.51 |
| | line broadening | $\Delta^{(0)}$ | 2.64 | 2.62 | 2.18 | 2.76 | 2.73 | 2.79 | 2.86 |
| | | W | 0.28 | 0.09 | 0.05 | 0.13 | 0.18 | 0.17 | 0.14 |
| Criteria Matrix | | $\Delta 2A$ [(a)] | 0.19 | 0.07 | 0.67 | 1.05 | 0.93 | 0.58 | 0.67 |

(a) $\Delta 2A = |2A_{eff}' - 2A_{eff}|$, where the $2A_{eff}'$ is measured from the simulated spectrum and the $2A_{eff}$ is directly measured from the experimental spectrum, in this case, $2A_{eff}$ = 65.92 Gauss

**Figure S6.3b:** Simulation of the 3U mutant spectrum obtained at 25 °C. (A) Comparison of the "lowest-$\chi^2$" spectra (dotted red) to that of the measured one (black). Each "lowest-$\chi^2$" spectrum was simulated with a fixed $C_{20}$ as indicated. (B) Simulation parameters and assessement matrics for "lowest-$\chi^2$" spectra shown in (A). Sets marked by "*" were deemed acceptable based on criteria described in S.6.3. The other sets either give $\Delta 2A > 0.30$ G, and/or show clear deviations at the high-field manisfold (inset), therefore were deemed not acceptable. Overall, the analyses indicate that for 3U ribozyme, $C_{20}$ must be smaller than 4 ($S \leq 0.71$), and correspondingly $\log_{10}(R_{bar}) \leq 7.32$.

**References**:


[1] K. Karbstein, J. Lee, D. Herschlag, *Biochemistry* **2007**, *46*, 4861-4875.
[2] N. Barhate, P. Cekan, A. P. Massey, S. T. Sigurdsson, *Angew. Chem. Int. Ed. Engl.* **2007**, *46*, 2655-2658.
[3] G. P. G. Grant, A. Popova, P. Z. Qin, *Biochem. Biophys. Res. Commun.* **2008**, *371*, 451-455.
[4] D. Herschlag, T. R. Cech, *Nature* **1990**, *344*, 405-409.
[5] a) G. J. Narlikar, M. Khosla, N. Usman, D. Herschlag, *Biochemistry* **1997**, *36*, 2465-2477; b) L. E. Bartley, X. Zhuang, R. Das, S. Chu, D. Herschlag, *J. Mol. Biol.* **2003**, *328*, 1011-1026.
[6] X. Shi, S. V. Solomatin, D. Herschlag, *J. Am. Chem. Soc.* **2012**, *134*, 1910-1913.
[7] a) N. R. Markham, M. Zuker, *Nuc. Acids Res.* **2005**, *33*, W577-W581; b) T. Xia, J. J. SantaLucia, M. E. Burkard, R. Kierzek, S. J. Schroeder, X. Jiao, C. Cox, D. H. Turner, *Biochemistry* **1998**, *37*, 14719-14735.
[8] D. S. Knitt, G. J. Narlikar, D. Herschlag, *Biochemistry* **1994**, *33*, 13864-13879.
[9] X. Zhang, P. Cekan, S. T. Sigurdsson, P. Z. Qin, *Method Enzymol.* **2009**, *469*, 303-328.
[10] K. A. Earle, D. E. Budil, in *Advanced ESR Methods in Polymer Reaserch* (Ed.: S. Schlick), John Wiley and Sons, New York, **2006**, pp. 53-83.
[11] T. M. Okonogi, A. W. Reese, S. C. Alley, P. B. Hopkins, B. H. Robinson, *Biophys. J.* **1999**, *77*, 3256-3276.
[12] L. E. W. LaConte, V. Voelz, W. Nelson, M. Enz, D. D. Thomas, *Biophys. J.* **2002**, *83*, 1854-1866.
[13] H. S. Mchaourab, M. A. Lietzow, K. Hideg, W. L. Hubbell, *Biochemistry* **1996**, *35*, 7692-7704.
[14] E. Meirovitch, M. Zerbetto, A. Polimeno, J. H. Freed, *J. Phys. Chem. B* **2011**, *115*, 143-157.
[15] a) Z. Zhang, M. R. Fleissner, D. S. Tipikin, Z. Liang, J. K. Moscicki, K. A. Earle, W. L. Hubbell, J. H. Freed, *J. Phys. Chem. B* **2010**, *114*, 5503-5521; b) L. Columbus, T. Kalai, J. Jeko, K. Hideg, W. L. Hubbell, *Biochemistry* **2001**, *40*, 3828-3846.